

## RESEARCH ARTICLE

10.1002/2017SW001743

## Key Points:

- We compared solar proton event onsets from neutron monitors and geostationary satellite observations on equal terms
- Neutron monitors and satellite observations yielded similar onset times, with the median onset time difference being 0 min

## Correspondence to:

J. V. Rodriguez,  
juan.v.rodriguez@colorado.edu

## Citation:

He, J., & Rodriguez, J. V. (2018). Onsets of solar proton events in satellite and ground level observations: A comparison. *Space Weather*, 16, 245–260. <https://doi.org/10.1002/2017SW001743>

Received 8 OCT 2017

Accepted 19 FEB 2018

Accepted article online 1 MAR 2018

Published online 23 MAR 2018

## Onsets of Solar Proton Events in Satellite and Ground Level Observations: A Comparison

Jing He<sup>1,2</sup>  and Juan V. Rodriguez<sup>3</sup> 

<sup>1</sup>Department of Physics, Middlebury College, Middlebury, VT, USA, <sup>2</sup>Now at Massachusetts Institute of Technology and Woods Hole Oceanographic Institute Joint Program in Oceanography and Applied Ocean Science and Engineering, Cambridge, MA, USA, <sup>3</sup>Cooperative Institute for Research in Environmental Sciences, University of Colorado Boulder, Boulder, CO, USA

**Abstract** The early detection of solar proton event onsets is essential for protecting humans and electronics in space, as well as passengers and crew at aviation altitudes. Two commonly compared methods for observing solar proton events that are sufficiently large and energetic to be detected on the ground through the creation of secondary radiation—known as ground level enhancements (GLEs)—are (1) a network of ground-based neutron monitors (NMs) and (2) satellite-based particle detectors. Until recently, owing to the different time resolution of the two data sets, it has not been feasible to compare these two types of observations using the same detection algorithm. This paper presents a comparison between the two observational platforms using newly processed  $>100$  MeV 1 min count rates and fluxes from National Oceanic and Atmospheric Administration's Geostationary Operational Environmental Satellite (GOES) 8–12 satellites, and 1 min count rates from the Neutron Monitor Database. We applied the same detection algorithm to each data set (tuned to the different background noise levels of the instrument types). Seventeen SPEs with GLEs were studied: GLEs 55–70 from Solar Cycle 23 and GLE 71 from Solar Cycle 24. The median difference in the event detection times by GOES and NM data is 0 min, indicating no innate benefit in time of either system. The 10th, 25th, 75th, and 90th percentiles of the onset time differences (GOES minus NMs) are  $-7.2$  min,  $-1.5$  min,  $2.5$  min, and  $4.2$  min, respectively. This is in contrast to previous studies in which NM detections led GOES by 8 to 52 min without accounting for different alert protocols.

### 1. Introduction

Solar proton events (SPEs) have been detected on the ground since the early 1940s and from space since the 1950s. From the earliest years, SPEs have been studied for practical reasons, owing to the ionospheric radio absorption they cause at high latitudes, as well as the radiation hazard they pose to humans and technology in space. SPE alert systems have been developed based separately on ground- and satellite-based observations that take advantage of the strengths of their respective measurements. Primary particles of solar or galactic origin that strike the top of the atmosphere cause cascades of secondary particles such as muons and neutrons (see, e.g., Lopate, 2006; Simpson et al., 1953) that can be detected on the ground if the primary population is sufficiently energetic. For example, primary protons must have kinetic energies of approximately  $>500$  MeV in order to cause detectable secondary neutrons on the ground; this effect is known as the atmospheric cutoff (e.g., Caballero-Lopez & Moraal, 2012; Clem & Dorman, 2000; Flückiger et al., 2008; Lopate, 2006; Mishev et al., 2013). The geomagnetic field (the internal field plus contributions from magnetospheric current systems) imposes an additional lower-rigidity (momentum per unit charge) cutoff on the primary population that increases with decreasing latitude, thus serving as a magnetic spectrometer that can be exploited with a network of ground-based neutron monitors (NMs) (Simpson et al., 1953). The geomagnetic field also controls access of solar and galactic ions to satellite orbit and has been used as a spectrometer in low-Earth orbit (e.g., Mazur et al., 1999), though not in geostationary orbit. In geostationary orbit, the geomagnetic cutoff energy depends on local time, magnetospheric activity, and detector look direction and, for protons, is generally below 100 MeV (well below that for westward looking detectors) (e.g., Kress et al., 2013; Rodriguez et al., 2010). Small satellite-borne detectors whose main purpose is the real-time monitoring of solar (as opposed to galactic) ion fluxes typically observe the primary solar proton population below  $\sim 1$  GeV, thereby complementing the spectral coverage of global NM networks (e.g., Matthiä, Heber, Reitz, Meier, et al., 2009; Matthiä, Heber, Reitz, Sihver, et al., 2009; Tylka & Dietrich, 2009). The  $>500$  MeV

components of especially energetic SPEs are observed as enhancements in NM count rates relative to the cosmic ray background, commonly referred to as ground level enhancements (GLEs) (e.g., Gopalswamy et al., 2012; Lopate, 2006; Shea & Smart, 2012). This paper compares the onset detection of “SPEs with GLEs” (Oh et al., 2010), also referred to as “GLE events” (Mewaldt et al., 2012; Souvatzoglou et al., 2014; Usoskin et al., 2011), by a network of ground-based NMs and by geostationary observations of solar protons above 100 MeV.

The onset of an SPE is generally observed as a sudden increase in instrument count rates above a noisy background level that is due to a combination of galactic cosmic ray (GCR) fluxes and instrument noise. Space weather alerts based on such arrivals contend with the problem of identifying event onsets in the presence of noise, balancing low false alarm rates and rapid issuance of alerts. (In this paper we follow the terminology of the National Oceanic and Atmospheric Administration (NOAA) Space Weather Prediction Center (SWPC), which sometimes differs from that of referenced papers. Warnings are based on predictions—in the case of solar proton fluxes, based in part on soft X-ray solar flare observations (e.g., Balch, 2008; Kahler et al., 2007, 2017; Núñez, 2011, 2015) or solar microwave radio bursts (e.g., Zucca et al., 2017), while alerts are based on observations of proton event onsets.) SPE alerts issued by SWPC are based on observations by the primary NOAA Geostationary Operational Environmental Satellite (GOES) for solar protons. SWPC currently issues alerts based on  $>10$  MeV and  $>100$  MeV integral fluxes reported on a 5 min cadence after the fluxes have remained above a set level for three consecutive 5 min averages. The  $>10$  MeV alerts are issued in the interest of the safety of humans and technological assets in space, while the  $>100$  MeV alerts (if triggered) are more relevant to the safety of airline passengers and crew (though far from ideally so) (Matthiä et al., 2015; Meier & Matthiä, 2014). For the latter application, alerts based on GLEs in NM count rates have been developed using 1 min cadence data from networks of NMs (e.g., Bieber et al., 2004; Kuwabara et al., 2006; Mavromichalaki et al., 2011; Souvatzoglou et al., 2014). At present, the NOAA alerts use data from only one GOES satellite, gaining confidence by waiting for three consecutive observations above a predetermined level before the alert is issued. In contrast, the alert method of Kuwabara et al. (2006) uses an increasing number of coincidences among multiple high-latitude ( $>55^\circ$ ) NMs to increase the confidence in the alerts, with three coincidences corresponding to the highest confidence alert level. Rapid alert times are particularly important in the case of rapidly rising GLE events, exemplified by GLE 69 of 20 January 2005 (Bombardieri et al., 2008; Mishev et al., 2011; Plainaki et al., 2007), in which the dose rates at aviation altitudes increased by as much as a factor of 250 above background (at southern polar latitudes) within 7 min after onset (Matthiä, Heber, Reitz, Meier, et al., 2009).

Kuwabara et al. (2006) and Souvatzoglou et al. (2014) compared automatic alerts issued on 1 min cadence NM network data with SWPC human-in-the-loop alerts based on 5 min cadence GOES  $>10$  and  $>100$  MeV fluxes. The delay of the SWPC alerts with respect to the NM-based alerts ranged from 8 to 52 min in these two studies. However, in order to eliminate false alerts, the SWPC alerts are issued only after three consecutive 5 min averaged observations above a flux threshold. This protocol therefore introduces at least a 10 min delay after the first detection, which is included in the delays determined by these studies. While the salient differences in the two alert protocols were noted by Kuwabara et al. (2006) and Souvatzoglou et al. (2014), these distinctions are often not mentioned when the results of these papers are quoted.

A comparison between NM-based and GOES-based detection of GLE events is called for that eliminates all differences except those innate to the measurements. Therefore, we performed such a comparison of GLE event onset times using 1 min data from NMs and GOES instruments for all GLEs from Solar Cycle 23 and GLE 71 from Solar Cycle 24. This comparison was made possible by the availability of 1 min NM data from the Neutron Monitor Database (NMDB) (Mavromichalaki et al., 2011), funded by the European Union, and the calculation of 1 min GOES proton rates and fluxes in the 100–1,000 MeV range as part of a NOAA National Centers for Environmental Information effort to process high-time-resolution data from the GOES 8–12 satellite series. The question posed is simple: How do GLE event onset times compare as determined from NM and GOES 1 min observations when a similar detection algorithm is used? We find that the median difference between onset times observed by NMs and GOES is 0 min. In section 2, we describe the data used in this study, in particular, the analyses used to create 1 min GOES data, and we illustrate the physical differences between the NM and GOES observations. We describe the onset detection method in section 3 and the results from applying this method to NM and GOES data in section 4. In section 5, we discuss the implications of our results for future real-time SPE alert systems.

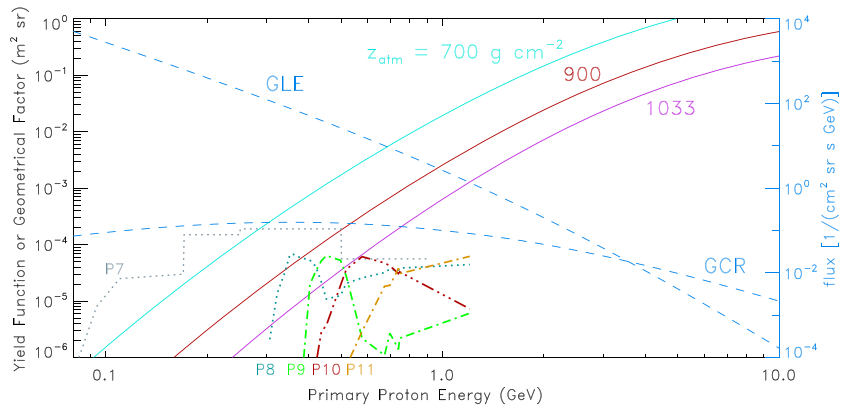


**Figure 1.** Comparison of 6-NM64 yield functions (Flückiger et al., 2008) for atmospheric depths ( $z_{\text{atm}}$ ) of 700, 900, and 1,033  $\text{g cm}^{-2}$  (solid lines), and the GOES P7–P11 geometrical factors (dotted and dash-dotted lines), both sets in units of  $\text{m}^2 \text{sr}$ . The GOES geometrical factors combine both front and rear entry responses. For reference, energy spectra (dashed lines) characteristic of ground level enhancement (GLE) 70 (Matthiä, Heber, Reitz, Sihver, et al., 2009) and of galactic cosmic rays (GCRs) near the end of 2006 (Matthiä et al., 2013) are plotted with reference to the right-hand axis.

## 2. Data

This study covers the GLEs (55–70) of Solar Cycle 23 (SC23) (Cliver, 2006; Gopalswamy et al., 2012; Mewaldt et al., 2012; Shea & Smart, 2012; see also <http://gle oulu.fi>), the first occurring on 6 November 1997 and the last on 13 December 2006 (Gopalswamy et al., 2012; Matthiä, Heber, Reitz, Sihver, et al., 2009; Plainaki et al., 2009a, 2009b), as well as GLE 71, which occurred on 17 May 2012 (Gopalswamy et al., 2013; Mishev et al., 2014; Plainaki et al., 2014). The NM data used in this study are restricted to pressure- and efficiency-corrected 1 min count rates from the NMDB (Mavromichalaki et al., 2011). The GOES 8–15 data are from the Energetic Particle Sensors (EPS) and High-Energy Proton and Alpha Detectors (HEPAD) (Hanser, 2011; Sellers & Hanser, 1996). The EPS data used here are from the two higher-energy dome detectors. In particular, channel P7 comes from Dome D5, which consists of two silicon detectors wired in parallel under an  $8.0 \text{ g cm}^{-2}$  copper moderator with a  $130 \times 60^\circ$  field of view (FOV). The  $130^\circ$  north-south extent of this FOV is centered on the equatorial plane, looking  $20^\circ$  off from the orbital or antiorbital direction. However, above 115 MeV, protons begin to penetrate the tungsten collimator, resulting in a nearly omnidirectional response (and therefore a larger geometrical factor) from 140 to 900 MeV (as shown in Figure 1) (Panametrics, 1980). P7 has effective energies from cross calibrations in the range 148–181 MeV that are valid for monotonically decreasing solar proton spectra (Bruno, 2017; Sandberg et al., 2014). Given the broad energy response of P7, these effective energies are not valid during the first several minutes of an SPE before the  $>100 \text{ MeV}$  protons have arrived and the spectrum is therefore increasing over part of the P7 energy range.

HEPAD is a solid state telescope comprised of two silicon detectors and a fused-silica Čerenkov radiator that illuminates a photomultiplier tube (PMT) (Rinehart, 1978; Sellers & Hanser, 1996). The telescope has a  $\sim 35^\circ$  half-angle conical FOV that looks radially outward in the equatorial plane (i.e., toward zenith). Triple coincidences between the silicon detectors and the PMT are used to define four coarse energy channels (P8–P11) with lower energies between 330 and 700 MeV (Table 1). While upper energies are frequently

**Table 1**  
GOES 8–12 Channels Used in This Paper and Parameters Defining Their Sampling in Time

Channel	Instrument	Nominal energy range (MeV)	Sample interval (s)	Duty factor (%)	Read-out delay (s)
P7	EPS Dome D5	110–900	10.24	50	1.536
P8	HEPAD	330–420	10.24	50	0.000
P9	HEPAD	420–510	10.24	50	0.000
P10	HEPAD	510–700	10.24	100	0.000
P11	HEPAD	$>700$	10.24	100	0.000

Note. Energy ranges are from Hanser (2011). The P7–P11 channels on GOES 13–15 are sampled every 32.768 s with 100% duty factor and uniform (2.048 s) read-out delay.

quoted for P8–P10 (as in Table 1), in fact these channels have significant responses above these energies, especially when the rear-entry response is incorporated into the geometrical factor (as shown in Figure 1). P9 is the least “integral” of the channels. The rear-entry response is important as the HEPAD fluxes calculated by NOAA are not corrected for it. The HEPAD proton responses were calibrated up to 1.3 GeV in a laboratory proton beam. The P8–P11 responses to atmospheric muons (cosmic ray secondaries) were also measured in the lab for zenith (front-entry) and nadir (rear-entry) views, thereby providing an estimate of the integral response for highly relativistic, minimum-ionizing particles (Panametrics, 1990).

The GOES 8–12 HEPAD channel fluxes have only been available in 5 min averages, and the EPS fluxes at no better than 1 min resolution. For this paper, the GOES 8–12 EPS P7 and HEPAD proton count rates have been processed at the highest time resolution from the raw data (Table 1), then averaged to 1 min resolution. While the basic HEPAD detector design has not changed, the time-sampling scheme has been different on each satellite series. The GOES 8–12 sample spacing is 10.24 s, with the accumulation period being 5.12 s or 10.24 s depending on the channel (Table 1). The time stamps being at the end of the sample, they are corrected by subtracting half the accumulation period, plus the delay from the end of the accumulation period to the read-out. Count rates are calculated by dividing the counts per sample by the accumulation period, then averaging the rates whose corrected timestamps fall within the minutes defined by the NM data. In contrast, GOES-13 and GOES-15 fluxes are produced routinely at 1 min resolution. They have been converted back to count rates for the analysis of GLE 71.

During SC23 and SC24, integral fluxes have been produced by SWPC at 5 min cadence in support of the real-time alerts. The >100 MeV integral fluxes at 1 min cadence used in this study are derived from the 1 min uncorrected GOES channel fluxes by removing a 4 h running average of the backgrounds, applying the contamination correction used in the current SWPC processing, and calculating the integral fluxes following the SWPC integral flux algorithm (see Appendix A of Rodriguez et al., 2017). We thus come as close as possible to what would have been available to SWPC during these events had the integral fluxes been calculated at 1 min cadence. GOES-8 fluxes are used for GLEs 55–64, GOES-11 fluxes for GLE 70, and GOES-13 fluxes for GLE 71. Because, during the period of GLEs 65–69, the GOES-11 satellite was spinning and the GOES-12 P6 and P7 channels had failed, a proxy >100 MeV data set was created from the GOES-12 P5 and GOES-11 P6 and P7 channels to minimize spin signatures of particle anisotropy in the high-time-resolution fluxes (Rodriguez et al., 2014). The eastward looking GOES-10 fluxes were avoided due to the possibility of geomagnetic cutoff effects, particularly in the P5 channel (Rodriguez et al., 2010); therefore, only one set of >100 MeV fluxes could be calculated for many of the SPEs with GLEs during this period. Given the broad energy response of P7, the derived >100 MeV fluxes are dominated by >500 MeV protons during the first several minutes of an SPE before the >100 MeV protons have arrived.

In order to understand the differences between the responses of the GOES instruments and the NMs to SPE and GCR spectra, it helps to compare the geometrical factors of the GOES instruments with the NM yield functions (e.g., Clem & Dorman, 2000; Flückiger et al., 2008; Lopate, 2006). These functions of energy or rigidity occupy analogous positions within the integral equations relating the primary proton spectrum to the observed count rate:

$$\text{rate} = \int_{E_{co}}^{\infty} G(E, z) j(E) dE, \quad (1)$$

where  $E$  is the incident proton energy,  $z$  is the atmospheric depth of the observatory,  $j(E)$  is the primary differential directional proton flux (protons/(m<sup>2</sup> sr s GeV)),  $G(E, z)$  is the yield function or geometrical factor (m<sup>2</sup> sr), and  $E_{co}$  is the cutoff energy. The use of the vertical cutoff energy is usually a sufficient approximation for NMs (Clem & Dorman, 2000). At geostationary orbit, while the cutoff energies can vary significantly across the angular response of the GOES instruments, they are usually well below the energies considered here (Kress et al., 2013). Geometrical factors of satellite-borne instruments (here defined to include efficiency effects) are solely functions of the instrument’s design (and the neighboring spacecraft structure). In addition to instrument characteristics, NM yield functions also depend on the atmospheric transport of the primary spectrum and the creation of the secondaries observed by the NM (e.g., neutrons and protons) and therefore are commonly parameterized in terms of atmospheric depth (e.g., Caballero-Lopez & Moraal, 2012; Clem & Dorman, 2000; Flückiger et al., 2008; Lopate, 2006; Mishev et al., 2013). The temperature sensitivity of several types of NMs has been characterized (Krüger et al., 2008). (While heavier primary nuclei such as those of

helium (Caballero-Lopez & Moraal, 2012) and iron (Lopate, 2001) can cause significant levels of NM count rates, protons dominate the primary ion population and cause most of the secondary count rates.)

In Figure 1, EPS P7 and HEPAD P8–P11 geometrical factors (Panametrics, 1990, 1995) are compared with yield functions of the standard 6-NM64 neutron monitor designed originally for the International Quiet Sun Year (Hatton & Carmichael, 1964). These yield functions are calculated at three atmospheric depths (700, 900, and 1,033 g cm<sup>-2</sup>) using the parameterized method of Flückiger et al. (2008). These atmospheric depths range from one characteristic of high-altitude stations to sea level. The total HEPAD front-entry geometrical factor has a maximum value of  $0.73 \times 10^{-4}$  m<sup>2</sup> sr and is nearly flat over the 0.4–1.2 GeV range (Hanser, 2011; Panametrics, 1990) while the NM yield functions rise steeply through this range and at 1.0 GeV are 1–2 order of magnitudes greater than the HEPAD geometrical factor, depending on the atmospheric depth. To illustrate the difference between SPE and GCR spectra, two energy spectra are shown over the same energy range. The greater spectrum is from near the beginning of GLE 70 (Matthiä, Heber, Reitz, Sihver, et al., 2009), while the other spectrum is characteristic of GCRs near the end of 2006 (model parameter  $W_{ACE} = 37.6$ ) (Matthiä et al., 2013). One consequence of combining these spectra and the instrument response functions is that the ratio of SPE count rates to GCR count rates is much greater in the GOES data than in the NM data. However, the NM GCR count rates are much greater than the GOES GCR count rates, resulting in a lower Poisson-noise background against which to detect GLEs in the NM data.

While NM data are typically produced and analyzed as count rates, GOES channel data are customarily produced as differential directional fluxes. In this paper, the GOES channel data are shown and analyzed as count rates in order to illustrate the differences in instrument sensitivity and the relative contrast between SPE and GCR signals in different energy ranges. The GOES >100 MeV fluxes are derived from three GOES channels and therefore have no equivalent count rates.

### 3. Methods: Determining GLE Event Onsets From NM and GOES Data

#### 3.1. General Onset Detection Method

Although this paper does not describe the development of an actual real-time detection system, the comparison of GLE event onsets in two sets of real-time observations is best done by the use of a real-time onset detection method such as that of Kuwabara et al. (2006). That way, the results reflect the challenge of detecting an event onset rapidly in real time in the presence of a noisy background. For the emphasis of this paper on real-time detection, this is preferable to a noncausal onset detection method such as that of Miroshnichenko et al. (2005), which identifies the onset as the intersection of the preevent background with an exponential fit to the initial rise of the event, and may be more robust to noise.

To compare NM and GOES detections of GLE event onsets on equal terms, we applied a slightly modified version of Kuwabara et al.'s (2006) onset detection method to not only the NM count rates but also the GOES count rates and >100 MeV integral fluxes. This way, any biases arising from differences in the detection algorithms are eliminated. The general idea behind Kuwabara et al.'s (2006) GLE detection method is to look for a percent increase in count rates  $I(\tau)$  above a continually updated baseline. Their algorithm is given by

$$I(\tau) = \left\{ \frac{1}{\tau_c} \sum_{t=\tau-\tau_c}^{\tau} N(t) \right\} / \left\{ \frac{1}{\tau_b} \sum_{t=\tau-\tau_0-\tau_b}^{\tau-\tau_0} N(t) \right\}, \quad (2)$$

where  $N(t)$  is the observed count rate,  $\tau_b$  is the baseline duration,  $\tau_0$  is the interval between the baseline and the current time  $\tau$ , and  $\tau_c$  is the averaging time period. An alarm occurs when  $I(\tau)$  exceeds a set threshold. Kuwabara et al. (2006) found the optimal values for  $\tau_b$ ,  $\tau_0$ , and  $\tau_c$  to be  $\tau_b = 75$  min,  $\tau_0 = 10$  min, and  $\tau_c = 3$  min, so we used those same values in this study. The only parameter we modified when applying equation (2) to the GOES count rates and >100 MeV integral fluxes was the alarm threshold because of the difference in scale and noise seen in the different data sets. These alarm thresholds are based off of multiple NM and satellite coincidences and are described below and summarized in Table 2.

While the  $I(\tau)$  thresholds for each instrument were determined by multisatellite and NM coincidences (see sections 3.2 and 3.3), the GLE event onset time is *not* dependent on multiple coincidences. We defined the event onset time as the timestamp of the first alarm that is followed by at least four consecutive alarms from a single NM station or GOES channel (e.g., P7 and P8). Two alarms are defined to be “consecutive” if they are

**Table 2**  
*Thresholds Signifying an Alarm When Using Equation (2) to Detect GLE Event Onsets From Different Types of Observations*

Type of observation	Threshold
NM count rates	1.04
GOES EPS count rates	1.58
GOES HEPAD count rates	2.39
GOES >100 MeV integral fluxes	11.0

*Note.* An alarm occurs when the normalized count rate  $I(\tau)$  from equation (2) exceeds the set threshold, and different thresholds are necessary since the noise in each data set varies greatly. The NM threshold is the value used by Kuwabara et al. (2006) for a three-station coincidence, the GOES EPS and HEPAD thresholds were chosen to be the lowest value that yielded zero false alarms for a two-satellite coincidence, while the GOES integral flux threshold is the lowest value that yielded zero false alarms for a single satellite (since a multiple-satellite coincidence was not possible for this data set).

separated by 5 min or less; however, most consecutive alarms are separated by only 1 min. The requirement that there need to be at least five consecutive alarms eliminates any false alarms in all three of the data sets used (NM count rates, GOES count rates, and >100 MeV integral flux) for the GLE events in this study. Our definition of the detected event onset time differs from the definitions used by Kuwabara et al. (2006) and Souvatzoglou et al. (2014), both of whom defined different levels of alarms based on the number of NMs that simultaneously detected the GLE. There were multiple difficulties associated with trying to compare multiple levels of alarms: for example, one challenge is that there are many NM stations around the world, but only two operational GOES satellites at any given time, so we would have had to decide what the “GOES equivalent” to a NM station would be. We felt that trying to compare different levels of alarms would not contribute much to our goal of objectively comparing the different instruments’ abilities to detect GLE event onsets, and we sought a simpler and clearer onset definition.

Therefore, our onset definition based on five consecutive alarms from a single station suits our purposes better because it (a) yields earlier onset times, and more importantly, (b) simplifies the comparison process by eliminating the need to try and compare different levels of alarms, which would only introduce excess arbitrary decisions. Again, we used a detection algorithm and thresholds that are suitable for real-time detection, the latter being based on three-NM station or two-satellite coincidences.

### 3.2. Detecting GLE Onsets From NM Data

Kuwabara et al. (2006) discovered that a threshold of  $I(\tau) = 1.04$  or a 4% increase above the baseline was the lowest possible threshold—which is preferable for generating earlier alarms—that yielded zero false alarms for a three-NM station coincidence (Kuwabara et al., 2006, Appendix B). We used their threshold of  $I(\tau) = 1.04$  and our onset criteria (five consecutive alarms in a single-NM station) to determine the NM GLE onsets. The NM onset times found with this method were verified against previously published onset times (Kuwabara et al., 2006; Souvatzoglou et al., 2014) and were found to be similar. The NM onset times differed from those by Kuwabara et al. (2006) by no more than 3 min, and the onset times differed from Souvatzoglou et al.’s (2014) single-station “GLE Alert” onset times by no more than 5 min with the exception of two events: GLE 63 had a 13 min difference, and GLE 70 had a 10 min difference.

### 3.3. Detecting GLE Event Onsets From GOES Data

When applying equation (2) to the GOES data, we kept the same values for  $\tau_b$ ,  $\tau_o$ , and  $\tau_c$ , but changed the  $I(\tau)$  threshold for signifying an alarm. Adjusting the threshold was necessary because the GOES data are significantly noisier than the NM data, so a threshold of 4% would have resulted in excessive false alarms. For instance, in Figure 2, which shows the GOES and NMs normalized count rates for all the GLEs of SC23, we can see that the GOES normalized count rates usually span a few orders of magnitude, whereas the NM normalized count rates typically have a range of less than 1 (with a couple of exceptions for particularly large GLE events). Hence, the normal range of noise in the GOES count rates easily exceeds the 4% threshold. In addition, separate thresholds were set for the EPS (P7) and HEPAD (P8–P11) since these two instruments are quite different in their energy ranges and behavior (see section 2 and Table 1).

When determining the threshold for the NM count rates, Kuwabara et al. (2006) found the lowest threshold that yielded zero false alarms for three simultaneous NM alarms for the nine GLEs they studied (GLEs 60–69, excluding 68). The three-NM coincidence criteria allowed them to set a lower threshold, which results in earlier alarms. We sought to emulate their standard by finding the lowest thresholds for the GOES EPS and HEPAD count rates that yielded zero false alarms for a two-satellite coincidence for all the GLE events of SC23, where a false alarm is defined as an isolated alarm that does not meet our onset definition from section 3.1. Because there are only two operational GOES satellites at any given time, we are limited to a two-satellite coincidence, whereas Kuwabara et al. (2006) were able to use a three-NM coincidence. For GLEs 55–57, GOES-8 and GOES-9 were used to determine the two-satellite coincidences; for GLEs 58–64, GOES-8 and GOES-10 were used; and for GLEs 65–70, GOES-10 and GOES-11 were used for the EPS count rates, but GOES-10 and GOES-12 were used for the HEPAD count rates. The different pairings for GLEs

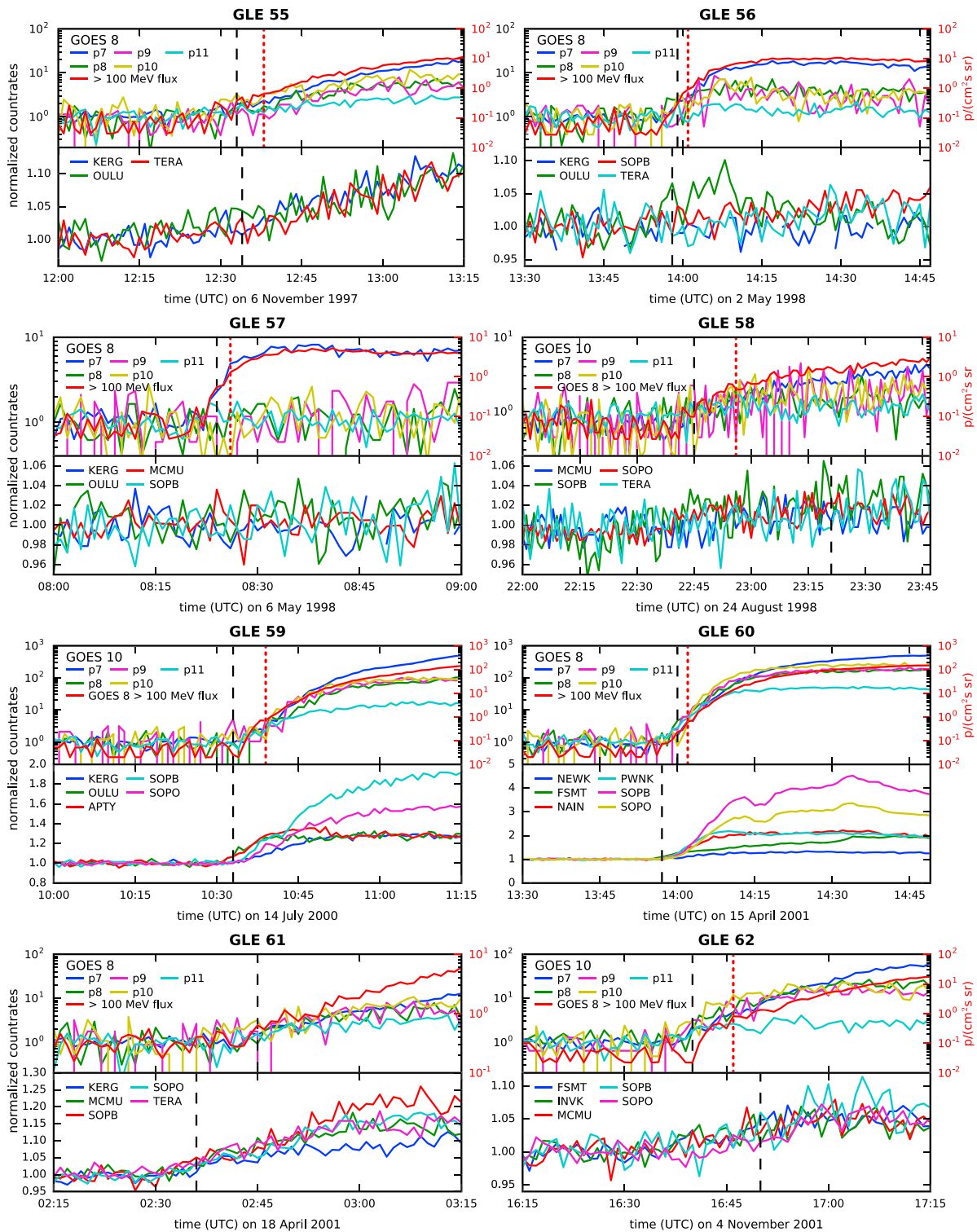


**Figure 2.** Time series of normalized 1 min count rates from neutron monitors (NMs) and GOES EPS and HEPAD channels, as well as 1 min >100 MeV integral fluxes (on the right axes in red) for each ground level enhancement (GLE) event of SC23. The count rates were normalized by dividing by an average baseline value calculated over a 75 min period starting at 85 min prior to the onset time. The event onset times detected by each instrument are indicated by a dashed black line, and the event onset times detected in the >100 MeV integral flux data are indicated by a red dotted line. For clarity, only select NMs (typically the first few stations that registered an alarm) are shown in the plots. Furthermore, for each GLE event, the GOES count rates are from whichever satellite had the earliest alarm. The >100 MeV fluxes are from GOES-8 for GLEs 55–64, a combination of GOES-11 and GOES-12 for GLEs 65–69 (as described in the text), and GOES-11 for GLE 70. Note that the GOES count rates are plotted on a log scale, while the NM count rates (with the exception of GLE 69) are not.

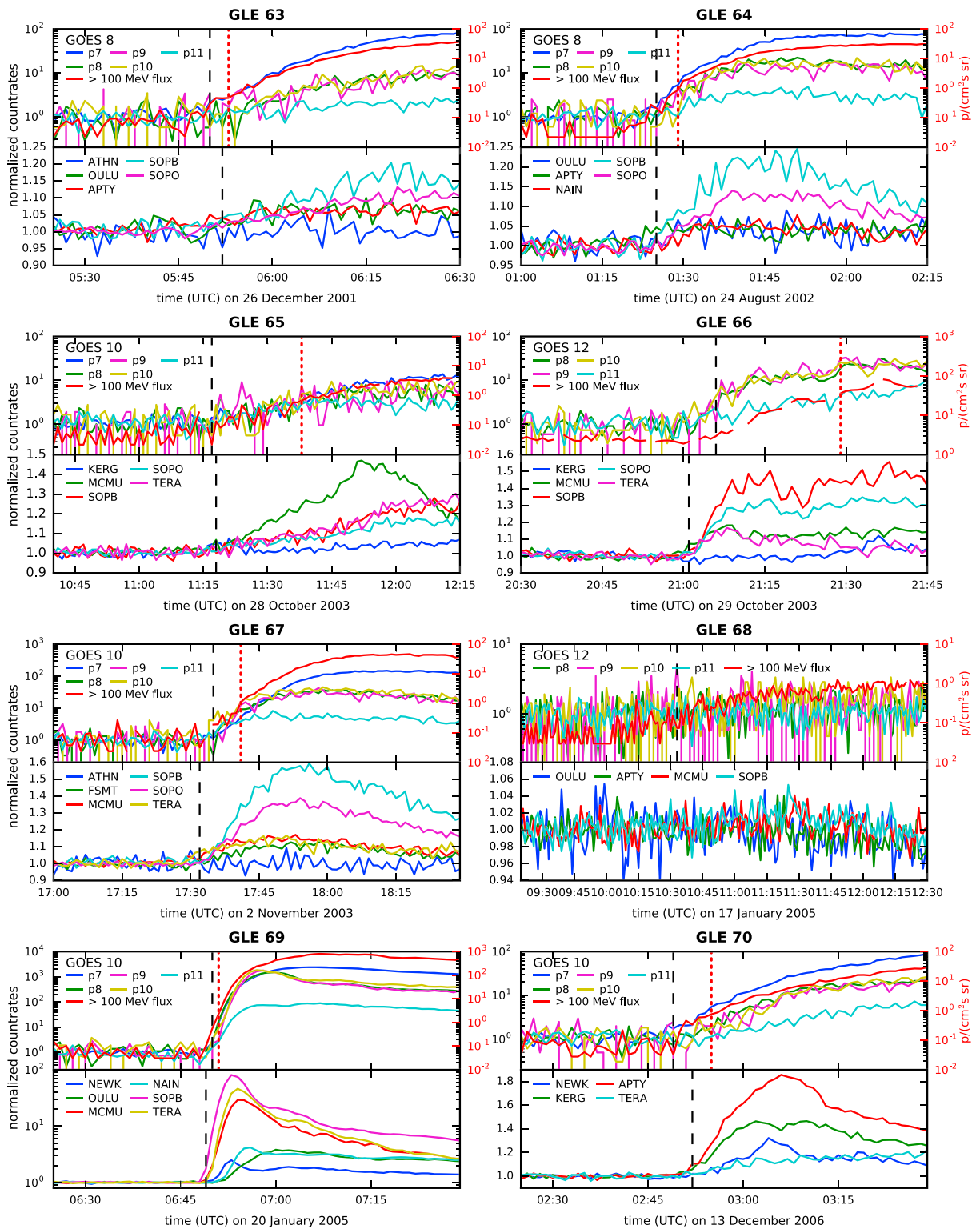


Figure 2. (continued)

**Table 3**
*List of GLE Events Studied in This Paper and Their Onset Times Detected by GOES Count Rates, >100 MeV Integral Fluxes, and NM Count Rates*

GLE	Date	GOES onset time (UTC)	100 MeV integral fluxes (UTC)	NM onset time (UTC)	GOES	NM stations
55	1997 Nov 6	12:33	12:38	12:34	8, 9	KERG, OULU, TERA
56	1998 May 2	13:59	14:01	13:58	8, 9	KERG, OULU, MCMU, SOPB, SOPO, TERA
57	1998 May 6	8:24	8:26	None detected	8, 9	KERG, OULU, MCMU, SOPB, SOPO, TERA
58	1998 Aug 24	22:45	22:56	23:21	8, 10	ESOI, OULU, MCMU, SOPB, SOPO, TERA
59	2000 Jul 14	10:33	10:39	10:33	8, 10	KERG, OULU, APTY, MCMU, SOPB, SOPO, TERA
60	2001 Apr 15	14:00	14:02	13:57	8, 10	ESOI, ATHN, AATB, NEWK, KERG, OULU, APTY, FSMT, MCMU, NAIN, PWNK, SOPB, SOPO, TERA
61	2001 Apr 18	2:45	None detected	2:36	8, 10	ESOI, ATHN, AATB, NEWK, KERG, OULU, APTY, FSMT, MCMU, NAIN, PWNK, SOPB, SOPO, TERA
62	2001 Nov 4	16:40	16:46	16:50	8, 10	ESOI, ATHN, AATB, NEWK, OULU, APTY, FSMT, INVK, MCMU, NAIN, PWNK, THUL, SOPB, SOPO, TERA
63	2001 Dec 26	5:50	5:53	5:52	8, 10	ESOI, ATHN, AATB, NEWK, OULU, APTY, FSMT, INVK, MCMU, NAIN, THUL, SOPB, SOPO, TERA
64	2002 Aug 24	1:25	1:29	1:25	8, 10	ESOI, ATHN, AATB, NEWK, KERG, OULU, APTY, FSMT, INVK, MCMU, NAIN, PWNK, THUL, SOPB, SOPO, TERA
65	2003 Oct 28	11:17	11:38	11:18	10, (11), 12	ESOI, ATHN, AATB, NEWK, KERG, OULU, APTY, FSMT, INVK, MCMU, NAIN, PWNK, THUL, SOPB, SOPO, TERA
66	2003 Oct 29	21:06	21:29	21:01	10, (11), 12	ESOI, ATHN, AATB, NEWK, KERG, OULU, APTY, FSMT, INVK, MCMU, NAIN, PWNK, THUL, SOPB, SOPO, TERA
67	2003 Nov 2	17:35	17:41	17:32	10, (11), 12	ESOI, ATHN, AATB, NEWK, KERG, OULU, APTY, FSMT, INVK, MCMU, NAIN, PWNK, THUL, SOPB, SOPO, TERA
68	2005 Jan 17	10:33	None detected	None detected	10, (11), 12	AATB, LMKS, NEWK, OULU, APTY, FSMT, INVK, MCMU, NAIN, PWNK, THUL, SOPB, SOPO
69	2005 Jan 20	6:50	6:51	6:49	10, (11), 12	ESOI, AATB, NEWK, KERG, OULU, APTY, FSMT, INVK, MCMU, NAIN, THUL, SOPB, SOPO, TERA
70	2006 Dec 13	2:49	2:55	2:52	10, 11, 12	ESOI, ATHN, AATB, NEWK, KERG, APTY, FSMT, INVK, MCMU, NAIN, PWNK, THUL, TERA
71	2012 May 17	1:57	1:59	1:55	13, 15	ATHN, MXCO, NANM, AATB, ROME, BKSJ, JUNG, JUNG1, LMKS, MCRL, NEWK, KIEL2, YKTK, KERG, OULU, APTY, TXBY, FSMT, INVK, NAIN, PWNK, THUL, SOPB, SOPO, TERA

*Note.* For each GLE event, the GOES satellites and NM stations from which data were used are listed. The parentheses around "11" indicate that the GOES 11 fluxes were used for calculating >100 MeV fluxes. The NM data for GLEs 55–70 were accessed in June 2016, while the NM data for GLE 71 were accessed January 2017. More information regarding the NM stations can be found in Table 4.

65–70 are due to the failure of the GOES-12 EPS P7 channel, but we otherwise avoided using GOES-11 because it was spinning during this time. See section 2 for more details.

This yielded the thresholds of  $I(\tau) = 1.58$  for the EPS count rates and  $I(\tau) = 2.39$  for the HEPAD count rates. The HEPAD data are noisier than the EPS P7 data, so it is expected that HEPAD has a higher threshold. Furthermore, the GOES-11 data were only included in the step where we determined the thresholds because GOES-11 was needed for a two-satellite coincidence in the EPS P7 channel for GLEs 65–70. The GOES-11 and GOES-12 P7 data were excluded from the analysis to determine the GOES GLE event onsets, however, for reasons explained in section 2.

**Table 4**  
List of NM Station Names and Latitudes Used in Table 3

NM station name	Abbreviation	Cutoff rigidity (GV)
Alma-Ata B	AATB	6.69
Apatity	APTY	0.65
Athens	ATHN	8.53
Baksan	BKSN	5.70
Emilio Segrè Obs. Israel	ESOI	10.75
Fort Smith	FSMT	0.30
Inuvik	INVK	0.30
IGY Jungfrauoch	JUNG	4.49
NM64 Jungfrauoch	JUNG1	4.49
Kerguelen	KERG	1.14
Kiel RT	KIEL2	2.36
Lomnický štít	LMKS	3.84
McMurdo	MCMU	0.30
Mobile Cosmic Ray Laboratory	MCRL	2.46
Mexico	MXCO	8.28
Nain	NAIN	0.30
Nor-Amberd	NANM	7.10
Newark	NEWK	2.40
Oulu	OULU	0.81
Peawanuck	PWNK	0.30
Rome	ROME	6.27
South Pole Bare	SOPB	0.10
South Pole	SOPO	0.10
Terre Adélie	TERA	0.01
Thule	THUL	0.30
Tixie Bay	TXBY	0.48
Yakutsk	YKTK	1.65

Note. Rigidities are from <http://www.nmdb.eu>.

Lastly, GLE event onsets were also determined from the >100 MeV 1 min integral flux data using the modified method of Kuwabara et al. (2006) with a threshold of  $I(\tau) = 11$ . As discussed above, only one set of >100 MeV fluxes without significant geomagnetic cutoff effects could be calculated for the entire period. Therefore, it was not possible to set the threshold for the >100 MeV integral flux data based on multiple-satellite coincidences, so this threshold was determined by simply finding the lowest threshold that resulted in no false alarms for the GLE events in this study.

The NM GLE onsets and EPS/HEPAD GLE event onsets were compared to evaluate the effects of the different instruments. Furthermore, to investigate any differences between using direct count rates and the >100 MeV integral fluxes, the >100 MeV integral flux event onsets were compared with the EPS P7 event onsets since the P8–P11 count rates are not used in the >100 MeV integral flux calculation (see Appendix A of Rodriguez et al., 2017). The P7 event onsets were calculated in the same way as the EPS/HEPAD onsets above, except we ignored the P8–P11 channels. Additionally, the integral flux onsets were only compared against the P7 onsets from the satellites that were used to calculate the integral fluxes: GOES-8 for GLEs 55–64, GOES-11 for GLEs 65–70, and GOES-13 for GLE 71.

#### 4. Results

The onset times for each GLE event as detected from NM and GOES count rates do not vary as much as was found in previous studies. Table 3 summarizes the onset times for each event determined from GOES EPS and HEPAD count rates, GOES >100 MeV integral fluxes, and NM count rates, and Figures 2 and 3 show the time series of the

three data sets used for each event in this study. The P7 rates and the >100 MeV fluxes have similar time series apart from the different units, as is expected since the latter are derived from the former.

##### 4.1. Comparing NM and GOES Count Rate Onsets

The median difference in the onset times between GOES count rates and NM data is 0 min, with the extremes being GOES detecting the onset 36 min ahead of NMs (GLE 58) and NMs detecting the onset 9 min ahead of GOES EPS/HEPAD (GLE 61). The 10th, 25th, 75th, and 90th percentiles of the onset time differences (GOES minus NM) are –7.2 min, –1.5 min, 2.5 min, and 4.2 min, respectively, where a negative value indicates that the GOES onset precedes the NMs onset.

In general, the largest GLE events exhibited smaller differences between the NM and GOES onset times, whereas the largest onset differences were found in the smaller events. The left-hand panel of Figure 4 shows a scatter plot of the NM and EPS/HEPAD onset differences for each GLE event versus the maximum normalized (to the preonset baseline) P7 count rate in the first 10 min post-GOES onset, which was used as a proxy for the initial rate of rise of the event. The P7 count rate was chosen as the proxy because it is the least noisy of the GOES channels while still having an upper cutoff of 900 MeV (Table 1). Although the relationship between the maximum P7 rates in the first 10 min and the GOES–NM onset differences is not simple, the largest delays are associated with the lowest maximum rates in P7, suggesting that the initial rate of rise has a significant effect on detectability.

Figure 4 shows that the largest GLE events (including GLEs 60 and 69) have onset differences of 3 min or less. Additionally, the only events that had onset differences greater than 5 min are GLEs 58, 61, and 62. GLEs 58 and 62 were weak events; the maximum count rate increase among all NMs in these two weak events was 4% for GLE 58 and 8% for GLE 62 (Usoskin et al., 2011). Furthermore, GLEs 57 and 68 were not detected in NM rates by our automatic method, but were detected in the GOES count rates. The maximum count rate increase in these two weak events was 4% for GLE 57 and 3.5% for GLE 68 (Usoskin et al., 2011). The NM

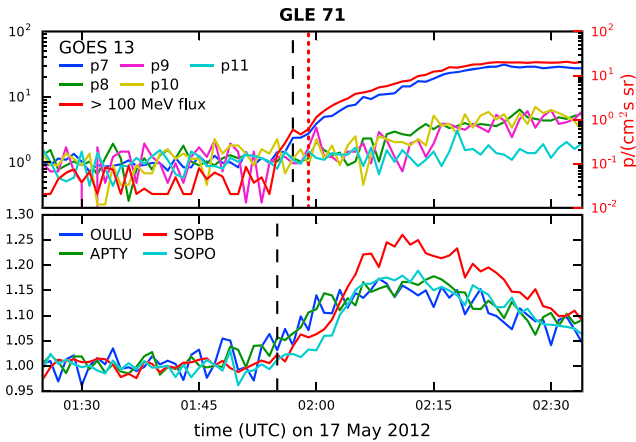


**Figure 3.** Same as Figure 2 but for GLE 71 from SC24. The neutron monitor stations shown were the only Neutron Monitor Database stations in whose data our method detected the onset of this GLE.

alarm threshold applied to the running quantity in equation (2) is 1.04 (Table 2). Clearly, a 4% increase lies on the borderline of detectability using our technique, depending on rise time and duration. In contrast, GLE 61 was much larger (26% increase, Usoskin et al., 2011), but the time series for this event shown in Figure 2 indicate that the 9 min delay between NM and GOES detection of this slowly rising event may be dominated by a physical difference rather than noise. The source for this event was beyond the solar limb, and therefore not magnetically well connected to the Earth (Reames, 2009), suggesting a propagation effect.

Given the average orientation of the interplanetary magnetic field (IMF) in the ecliptic plane (Parker spiral angle) of about 45° from the Sun-Earth line, one might expect GOES satellites between dawn and noon to detect GLE event onsets earlier relative to other local times. Therefore, in the right-hand panel of Figure 4, the GOES-NM onset differences are plotted against the local time of the GOES satellite at the time of detection of the GLE, the assumption being that, since NMs are located all over the world, there is a NM that has an asymptotic look direction

close to the direction of arrival at any given time. The maximum normalized P7 rate in the first 10 min post-onset is represented by the color scale. Figure 4 shows no obvious relationship between the onset differences and the local time. This is not surprising for several reasons. The IMF orientation can depart substantially from the average, such as in the presence of an interplanetary coronal mass ejection or corotating interaction region, and moreover the GLE anisotropy axis often departs tens of degrees from the IMF orientation measured at a point near Earth (e.g., Bieber et al., 2002, 2005; Bombardieri et al., 2008; Miroshnichenko et al., 2005; Mishev et al., 2014; Plainaki et al., 2007, 2014). In any case, however, the 1 min resolution of the data probably precludes the possibility of resolving any systematic local time dependence, given the velocities of these relativistic protons.

#### 4.2. Comparing GOES P7 Count Rate Onsets and >100 MeV Integral Flux Onsets

All of the GLE event onsets determined from the >100 MeV integral fluxes lag those detected from NM and GOES count rates. The median difference between the GOES >100 MeV integral flux onsets and the P7 count

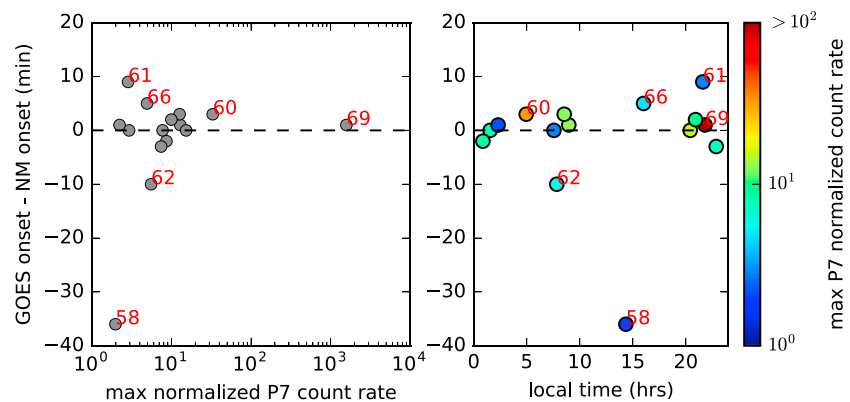


**Figure 4.** (left) Differences between Geostationary Operational Environmental Satellite (GOES) and neutron monitor (NM) onset times plotted against the maximum normalized P7 count rate in the first 10 min post-GOES onset, which was used as a proxy for the initial rate of rise of the event. (right) Differences between GOES and NM onset times plotted against the local time of the GOES satellite. Each point is colored by the maximum normalized P7 count rate that serves as the independent variable in the left-hand plot. The normalization method is described in the Figure 2 caption. The black dashed line indicates the median of the onset differences, which is 0 min. Some of the points are labeled by the corresponding ground level enhancement (GLE) number. For GLE 66, the P7 count rate used is from GOES-10 because GOES-11 was spinning and there was a P7 channel failure in GOES-12 (see section 2). Also note that GLEs 57 and 68 are omitted in this figure because they were not detected by NMs using our method.

rates onsets (flux minus P7 onsets) is 3 min, with the integral fluxes onsets lagging the P7 onsets. The 10th, 25th, 75th, and 90th percentiles of the onset differences are 2 min, 2 min, 4.5 min, and 13 min, respectively. The minimum onset difference is 1 min, which occurred in GLE 69, and the maximum difference 20 min, in GLE 65. This is consistent with the trend seen in the NM and GOES comparisons in section 4.1 that larger GLE events yield smaller onset differences while smaller GLE events have a larger onset difference. Furthermore, GLEs 61 and 68 went undetected in the  $>100$  MeV integral fluxes, their rises being too slow or too weak to be detected with our method using fluxes from a single satellite. Given the similarity between the P7 and  $>100$  MeV time series in Figures 2 and 3, this comparison indicates the benefit of using coincidences between SPE observations by the two operational GOES satellites to reduce the delay between event onset and alert issuance.

## 5. Discussion

The application of the same detection algorithm to 1 min NM and GOES count rates has revealed that the onsets of GLE events can be detected similarly well by these two very different systems and that their capabilities tend to be more similar as the initial rate of rise of the event increases. This tendency is illustrated in Figure 4. As seen in Figure 2, GLE 69 was the only event that exhibited orders-of-magnitude increase in the NM count rates; the difference between the GOES and NM detection times in this event was very small (+1 min, NMs leading GOES). For the next three largest GLEs—Easter 2001 (GLE 60), Bastille Day 2000 (GLE 59), and the last GLE in SC23 (GLE 70)—the onset time differences between the GOES and NM detections (GOES minus NMs) were +3, 0, and  $-3$  min, respectively.

At the other end of the scale, the 2% enhancement at South Pole in GLE 68 was too small to be detected by Kuwabara et al. (2006), although Souvatzoglou et al. (2014) identified an onset time of 0952 UT at Apatity and Gopalswamy et al. (2012) identified an onset time of 0955 UT at Oulu (3% enhancement). Using these stations plus McMurdo, our method did not detect GLE 68 in NM data. Nor did our method detect the event onset in the slowly rising  $>100$  MeV GOES fluxes (because  $I(\tau)$  did not exceed  $\sim 5.7$ ), although clearly these fluxes started to rise around 1000 UT (Figure 2), just after the brief enhancements in the NM data detected by the authors referenced above. However, our algorithm did identify an event onset at 1033 UT in GOES-12 HEPAD P9 count rates. Because it looks like a spike in the 1 min data, it is tempting to identify this as a false positive. However, this spike is not an artifact, and an analysis of the Poisson statistics of P9 indicates that it may have been a statistical fluctuation whose likelihood increased due to the event onset. From 0 to 10 UT on this day, the average Poisson  $\lambda$  (product of rate and accumulation period) in the GOES-12 P9 channel was 0.2520, and P9 registered three counts (in 5.12 s) only 6 times (out of a total of 3,516 observations), and no greater counts, consistent with this  $\lambda$ . Between 10 and 12 UT, during the weak event precursor, P9 registered three or more counts 6 times, including one contributor to the spike at 1033 UT, although the rate for the previous 10 h would have predicted 1.2 such events. This suggests that the detected spike was more likely to occur during the precursor. Nonetheless, forecasters probably would have dismissed such a spike as a false positive. In any case, this detection and those reported in the literature identify weak precursors to the main event, which started  $\sim 1200$  UT and peaked  $\sim 1700$  UT, as observed by EPS P7 and HEPAD P8–P11.

In the earlier work, the largest delay reported between the NM-based detections and the SWPC alerts is the 52 min delay for GLE 71 (Souvatzoglou et al., 2014). SWPC issued a  $>100$  MeV proton alert with a begin time of 0252 UT on 17 May 2012. In the present work, the event was detected using the NMs at 0155 UT, using the GOES count rates at 0157 UT, and using the GOES  $>100$  MeV flux at 0159 UT (Table 3). These small delays using a consistent method with data of the same time resolution, plus the clear signatures in the data (Figure 3), show that the large delay in the SWPC-issued alert was not due to innate properties of the GOES observations.

Some part of the timing differences may be attributable to spectral variations between events. SPE intensity and spectral hardness both affect the size of GLEs. Oh et al. (2010) showed that GOES EPS/HEPAD channels P5–P10 all exhibit a threshold in peak intensity, and in 12 h fluence following the event peak, above which the majority of events (during 1986–2006) are associated with GLEs. In a study of SC23 GLE events, Mewaldt et al. (2012) showed that the ratio of the peak GLE percent increase (above the GCR background) to the event-integrated 0.04–400 MeV energy content is strongly anticorrelated with the power law exponent at tens to hundreds of MeV ( $-\gamma_2$ ), with the largest ratio being associated with the hardest spectra. In Figure 5,

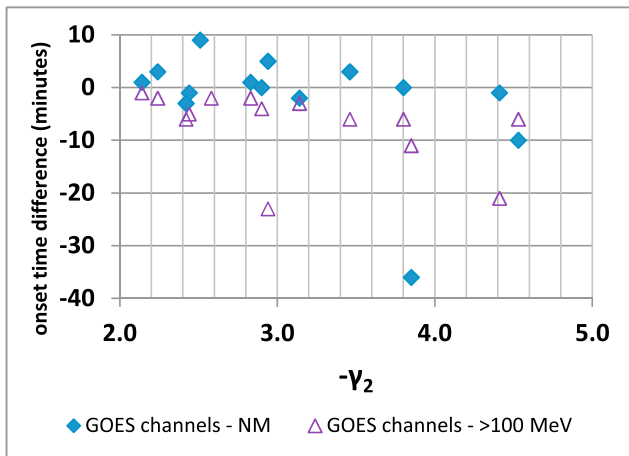


**Figure 5.** Ground level enhancement (GLE) event onset time differences from Table 3 versus power law exponents from Table 1 of Mewaldt et al. (2012). Two sets of differences are shown: those between the earliest of the Geostationary Operational Environmental Satellite (GOES) P7–P11 channels and the neutron monitor stations, and those between the earliest of the GOES channels and the >100 MeV flux.

we have compared the  $-\gamma_2$  from Table 1 of Mewaldt et al. (2012) with time differences in detected onsets from our Table 3. Two sets of differences are shown. Both sets, those between the earliest of the GOES P7–P11 channels and the NM stations, and those between the earliest of the GOES channels and the >100 MeV flux, exhibit a rather weak relationship between increasing delays and softer spectra. In the GOES–NM set, the most positive difference (NM ahead of GOES, GLE 61, 9 min) was associated with a hard spectrum ( $-\gamma_2 = 2.51$ ) while the most negative difference (GOES ahead of NM, GLE 58, –36 min) was associated with a soft spectrum ( $-\gamma_2 = 3.85$ ). In the second set, the most negative difference (GOES channels ahead of >100 MeV, GLE 66, –23 min) is an outlier from the general trend, being associated with a moderately hard spectrum ( $-\gamma_2 = 2.84$ ). With the caution that spectral hardness can vary significantly during an event, we conclude that event spectral hardness has some effect on onset detection differences, though other factors such as the initial rate of rise (affecting the signal and therefore the counting statistics in the channels being analyzed) also play a role.

The significance of the timing differences is better understood in the context of energetic proton travel times from the Sun. The propagation path length ranges from the nominal Parker spiral length of 1.2 astronomical units (AU) to as long as 2.5 AU (Reames, 2009). For this range

of path lengths, the difference in arrival times between 100 and 1,000 MeV protons ranges from 12 to 25 min. Probably, the key reason that such a systematic difference is not observed in the present comparisons between NM and GOES data is the strong response of the GOES P7 channel up to 900 MeV (Figure 1). A GLE event onset in the P7 fluxes and in the >100 MeV fluxes derived from them is probably dominated by >500 MeV protons. Similarly, for this range of path lengths, the difference in arrival times between 500 and 1,000 MeV protons ranges from 1.8 to 3.7 min. Such differences are well within the 10th to 90th percentile range of the results of the current paper. While the 12–25 min difference between 100 and 1,000 MeV protons lies within the 8–52 min range of delays between SWPC alerts and the NM-based alerts reported by Kuwabara et al. (2006) and Souvatzoglou et al. (2014), these studies compared the SWPC alerts, which use 5 min data, to NM alerts based on 1 min data and did not correct for the >10 min delay inherent in the SWPC alerts. If there is a perception in the community that the comparisons of Kuwabara et al. (2006) and Souvatzoglou et al. (2014) represent innate differences between NM and GOES detections of GLE event onsets above 100 MeV, rather than artifacts of different alert protocols, it may rest upon intuition derived from travel time considerations like this.

The near parity in the delays for the satellite- and NM-based observations should not be taken as rationale for using only one source. Rather, interoperability of satellite- and NM-based alerts should be the goal. An alert system with adequate safeguards against false alerts could be developed based on both NM and GOES real-time observations at 1 min cadence. For those large SPEs that cause significant GLEs, if an additional ~10 min of warning is important (Figure 4), then a real-time detection system that ingests data from satellites and NMs would be more robust to noise in the observations as well as spectral variations. Beyond onset detection, the satellite- and NM-based observations are complementary in their applicability. Among large SPEs, the component that causes GLEs is highly variable in intensity (e.g., Mewaldt et al., 2012; Oh et al., 2010). Therefore, use of satellite observations at lower energies can lead to false alarms of radiation exposure at aviation altitudes, as well as false negatives (Meier & Matthiä, 2014). The anisotropy observed during the initial phase of GLEs, which is an important input to accurate dose rate warnings (e.g., Matthiä, Heber, Reitz, Meier, et al., 2009; Matthiä, Heber, Reitz, Sihver, et al., 2009), currently can only be quantified using a NM network. In Figures 2 and 3, a salient distinction between the NM and GOES signatures is the presence of early maxima observed at one or more NM stations that are notably absent from the GOES observations (with the exception of GLE 69). Examples include most notably GLEs 56 (Oulu), 59 (Apatity and Oulu), 60 (South Pole and Peawanuck), 64 (South Pole), 65 (McMurdo), 66 (South Pole), 67 (South Pole, McMurdo, Terre Adelie, and Fort Smith), 69 (South Pole, Terre Adelie, McMurdo, Nain, and Newark), 70 (Apatity, Kerguelen, and Newark), and 71 (South Pole, Apatity, and Oulu). Such peaks and the anisotropies of which they are a signature have

### Acknowledgments

Thank you to the NOAA Ernest F. Hollings Scholarship for the opportunity to conduct this work. We thank L. Matheson for the software used to read the raw GOES 8–12 telemetry, and W. Denig for supporting the effort within the NOAA National Centers for Environmental Information (NCEI) to rescue these raw data. We also thank D. Matthiä for providing the software for his GCR model. T. Onsager provided comments on an earlier version of this manuscript. The high-resolution GOES 8–12 data used in this work are available upon request. The GOES 13–15 data are available from <https://www.ngdc.noaa.gov/stp/satellite/goes/dataaccess.html>. This study was partially supported by NOAA grant NA15OAR4320137 (Cooperative Institute for Research in Environmental Sciences) at the University of Colorado. We acknowledge the NMDB database ([www.nmdb.eu](http://www.nmdb.eu)), founded under the European Union's Seventh Framework (FP7) Programme (FP/2007-2013) under contract 213007, for providing data. The operation of the Alma-Ata neutron monitor is supported by the Institute of Ionosphere, Kazakhstan. Athens neutron monitor data were kindly provided by the Physics Department of the National and Kapodistrian University of Athens. Apatity neutron monitor data were kindly provided by the Polar Geophysical Institute. The Pushkov Institute of Terrestrial Magnetism, Ionosphere and radio wave propagation (IZMIRAN) kindly provided the Baksan and the Mobile Cosmic Ray Laboratory data. The operation of the Emilio Segrè Observatory neutron monitor is supported by ISA Ministry of Science of Israel, FP-7 "NMDB" grant, Tel Aviv University. The operation of the Jungfraujoch neutron monitors is supported by the Physikalisches Institut of the University of Bern and by the International Foundation High Altitude Research Stations Jungfraujoch and Gornergrat (HFSJG), CH-3012 Bern, Switzerland. Kerguelen and Terre Adélie neutron monitor data were kindly provided by the French Polar Institute (IPEV, Brest) and by Paris Observatory. The neutron monitor at Kiel (Germany) is operated by the Extraterrestrial Physics Department of the Institute for Experimental and Applied Physics of the Christian-Albrechts University of Kiel. The operation of the Lomnický štít neutron monitor is supported by Slovak grant agency APVV, project 51-053805. Mexico City neutron monitor data were kindly provided by the Cosmic Ray Group, Geophysical Institute, National Autonomous University of Mexico (UNAM), Mexico. The operation of the Nor-Amberd neutron monitor is

been studied by many authors (e.g., Bieber et al., 2002, 2004, 2005; Bombardieri et al., 2008; Eroshenko et al., 2004; Lopate, 2006; Matthiä, Heber, Reitz, Meier, et al., 2009; Matthiä, Heber, Reitz, Sihver, et al., 2009; Miroshnichenko et al., 2000, 2005; Mishev et al., 2014; Plainaki et al., 2007, 2014). These early peaks have some effect on the timing results, but more importantly they are evidence of the pronounced early anisotropy that a NM network can detect and that GOES cannot. On the other hand, satellite-based observations are needed in order to detect the majority of large SPEs that do not cause significant GLEs yet still pose a significant radiation hazard to satellites and humans in space as well as enhanced ionospheric absorption of high-frequency radio communications in the polar regions (Sauer & Wilkinson, 2008).

With SC24 proceeding toward minimum, it is likely that any such combined alert system would first come into use in SC25. By that time, EPS and HEPAD may no longer be in operation. On GOES-16 and later satellites, EPS and HEPAD are replaced by a new Solar and Galactic Proton Sensor (SGPS) (Dichter et al., 2015). SGPS provides improved spectral sampling above 100 MeV, including a >500 MeV integral channel, and the >100 MeV fluxes will be derived from the new channels using an algorithm described by Rodriguez et al. (2017). The SGPS channel rates are sampled every second and grouped in 1 min files transmitted in real time every minute. Since both operational GOES satellites (East and West) will continue to fly solar proton detectors, coincidences between SPE onsets observed at both satellites could be used to increase confidence in early onset detections, something that is not done at present with GOES data but is done with data from multiple NM stations.

## 6. Conclusions

We compared GLE event onset times as detected from NMs and GOES observations on equal terms by using data with the same time resolutions, the same detection algorithm, and the same onset definitions. We modified and applied the onset detection algorithm developed by Kuwabara et al. (2006)—which looks for a percent increase in count rates over a continuously updated baseline—to 1 min cadence NM and GOES count rates, as well as 1 min cadence GOES >100 MeV integral fluxes. The thresholds that signify an alarm are modified for each of the observations to account for differences in noise between different instruments' data and were set to be 1.04 for NM count rates, 1.58 for GOES EPS count rates, 2.39 for GOES HEPAD count rates, and 11 for GOES >100 MeV integral fluxes. These thresholds are based on three-NM coincidences, two-satellite coincidences for the GOES EPS and HEPAD channel count rates, and a single satellite for the >100 MeV fluxes. Two-satellite coincidences would be appropriate for a system with two operational satellites, while the threshold used on the >100 MeV fluxes reflects the current practice of using a single GOES satellite for SPE alerts.

Seventeen GLE events were studied from GLE 55 on 6 November 1997 to GLE 71 on 17 May 2012, and the median difference in the detection time between NM and GOES count rates was 0 min. The range of the (GOES minus NM) onset differences was –36 min (GOES preceded NMs) to +9 min (NM preceded GOES), with the 10th, 25th, 75th, and 90th percentiles being –7.2 min, –1.5 min, +2.5 min, and +4.5 min, respectively. In general, larger absolute onset differences were associated with the weaker events, whereas both NMs and GOES detected the larger events around the same time. No apparent local time dependence was found in the GOES onsets. The difference between GOES EPS P7 and GOES >100 MeV detections ranged from 1 to 20 min, with a median of 3 min, indicating the benefit of using coincidences between two geostationary satellites. We conclude that there is no significant difference in the innate ability of NM- and satellite-based systems to detect the onset of GLE events, which is contrary to previous studies comparing the two types of observations that found a bias toward NMs leading GOES by 8–52 min. This result indicates that the highest confidence in alerts of GLE event onsets would arise from a combination of multiple-satellite and multiple-NM observations, each of which contributes different strengths to the detection of SPEs.

## References

- Balch, C. C. (2008). Updated verification of the Space Weather Prediction Center's solar energetic particle prediction model. *Space Weather*, 6, S01001. <https://doi.org/10.1029/2007SW000337>
- Bieber, J. W., Clem, J., Evenson, P., Pyle, R., Ruffolo, D., & Sáiz, A. (2005). Relativistic solar neutrons and protons on 28 October 2003. *Geophysical Research Letters*, 32, L03502. <https://doi.org/10.1029/2004GL021492>
- Bieber, J. W., Dröge, W., Evenson, P. A., Pyle, R., Ruffolo, D., Pinsky, U., et al. (2002). Energetic particle observations during the 2000 July 14 solar event. *The Astrophysical Journal*, 567(1), 622–634.

supported by the Yerevan Physics Institute, Yerevan, Armenia. Oulu neutron monitor data were kindly provided by the Sodankyla Geophysical Observatory. Rome neutron monitor data were kindly provided by the Physics Department "E. Amaldi" of "Roma Tre" University. The Institute of Cosmophysical Research and Aeronomy, Russian Academy of Science kindly provided the Tixie Bay and Yakutsk data. The neutron monitor data from Fort Smith, Inuvik, Nain, Newark, Peawanuck, and Thule are provided by the University of Delaware Department of Physics and Astronomy and the Bartol Research Institute. The data from McMurdo were provided by the University of Delaware with support from the U.S. National Science Foundation under grant ANT-0739620. The data from South Pole and South Polar Bares are provided by the University of Delaware with support from the U.S. National Science Foundation under grant ANT-0838839.

- Bieber, J. W., Evenson, P., Dröge, W., Pyle, R., Ruffolo, D., Rujivarodom, M., et al. (2004). Spaceship Earth observations of the Easter 2001 solar particle event. *The Astrophysical Journal*, *601*(1), L103–L106.
- Bombardieri, D. J., Duldig, M. L., Humble, J. E., & Michael, K. J. (2008). An improved model for relativistic solar proton acceleration applied to the 2005 January 20 and earlier events. *The Astrophysical Journal*, *682*(2), 1315–1327.
- Bruno, A. (2017). Calibration of the GOES 13/15 high-energy proton detectors based on the PAMELA solar energetic particle observations. *Space Weather*, *15*, 1191–1202. <https://doi.org/10.1002/2017SW001672>
- Caballero-Lopez, R. A., & Moraal, H. (2012). Cosmic-ray yield and response functions in the atmosphere. *Journal of Geophysical Research*, *117*, A12103. <https://doi.org/10.1029/2012JA017794>
- Clem, J. M., & Dorman, L. I. (2000). Neutron monitor response functions. *Space Science Reviews*, *93*, 1–24.
- Cliver, E. W. (2006). The unusual relativistic solar proton events of 1979 August 21 and 1981 May 10. *The Astrophysical Journal*, *639*(2), 1206–1217.
- Dichter, B. K., Galica, G. E., McGarity, J. O., Tsui, S., Golightly, M. J., Lopate, C., et al. (2015). Specification, design and calibration of the space weather suite of instruments on the NOAA GOES-R program spacecraft. *IEEE Transactions on Nuclear Science*, *62*(6), 2776–2783.
- Eroshenko, E., Belov, A., Mavromichalaki, H., Mariatos, G., Oleneva, V., Plainaki, C., & Yanke, V. (2004). Cosmic-ray variations during the two greatest bursts of solar activity in the 23rd solar cycle. *Solar Physics*, *224*(1–2), 345–358.
- Flückiger, E. O., Moser, M. R., Pirad, B., Bütikofer, R., & Desorgher, L. (2008). A parameterized neutron monitor yield function for space weather applications. In R. Caballero, et al. (Eds.), *30th Proceedings International Cosmic Ray Conference 2007* (Vol. 1, pp. 289–292). Mexico City, Mexico: Universidad Nacional Autónoma de México.
- Gopalswamy, N., Xie, H., Akiyama, S., Yashiro, S., Usoskin, I. G., & Davila, J. M. (2013). The first ground level enhancement event of solar cycle 24: Direct observation of shock formation and particle release heights. *The Astrophysical Journal*, *765*(2), L30–L34. <https://doi.org/10.1088/2041-8205/765/2/L30>
- Gopalswamy, N., Xie, H., Yashiro, S., Akiyama, S., Mäkelä, P., & Usoskin, I. G. (2012). Properties of ground level enhancement events and the associated solar eruptions during solar cycle 23. *Space Science Reviews*, *171*(1–4), 23–60. <https://doi.org/10.1007/s11214-012-9890-4>
- Hanser, F. A. (2011). EPS/HEPAD calibration and data handbook (Tech. Rep. GOESN-ENG-048D). Carlisle, MA: Assurance Technology Corporation. Retrieved from <http://www.ngdc.noaa.gov/stp/satellite/goes/documentation.html>
- Hatton, C. J., & Carmichael, H. (1964). Experimental investigation of the NM-64 neutron monitor. *Canadian Journal of Physics*, *42*(12), 2443–2472. <https://doi.org/10.1139/p64-222>
- Kahler, S. W., Cliver, E. W., & Ling, A. G. (2007). Validating the proton prediction system (PPS). *Journal of Atmospheric and Solar - Terrestrial Physics*, *69*(1–2), 43–49. <https://doi.org/10.1016/j.jastp.2006.06.009>
- Kahler, S. W., White, S. M., & Ling, A. G. (2017). Forecasting E > 50-MeV proton events with the proton prediction system. *Journal of Space Weather and Space Climate*, *2017*, A27. <https://doi.org/10.1051/swsc/2017025>
- Kress, B. T., Rodriguez, J. V., Mazur, J. E., & Engel, M. (2013). Modeling solar proton access to geostationary spacecraft with geomagnetic cutoffs. *Advances in Space Research*, *52*(11), 1939–1948.
- Krüger, H., Moraal, H., Bieber, J. W., Clem, J. M., Evenson, P. A., Pyle, K. R., et al. (2008). A calibration neutron monitor: Energy response and instrumental temperature sensitivity. *Journal of Geophysical Research*, *113*, A08101. <https://doi.org/10.1029/2008JA013229>
- Kuwabara, T., Bieber, J. W., Clem, J., Evenson, P., & Pyle, R. (2006). Development of a ground level enhancement alarm system based upon neutron monitors. *Space Weather*, *4*, S10001. <https://doi.org/10.1029/2006SW000223>
- Lopate, C. (2001). Climax neutron monitor response to incident iron ions: An application to the 29 Sept 1989 ground level event, *Proc. 27th Int'l Cosmic Ray Conf. (Hamburg)*, *8*, 3398.
- Lopate, C. (2006). Fifty years of ground level solar particle event observations. In *Solar Eruptions and Energetic Particles, Geophysical Monograph Series 165* (pp. 283–296). Washington, DC: American Geophysical Union.
- Matthiä, D., Berger, T., Mrigakshi, A. I., & Reitz, G. (2013). A ready-to-use galactic cosmic ray model. *Advances in Space Research*, *51*(3), 329–338.
- Matthiä, D., Heber, B., Reitz, G., Meier, M., Sihver, L., Berger, T., & Herbst, K. (2009). Temporal and spatial evolution of the solar energetic particle event on 20 January 2005 and resulting radiation doses in aviation. *Journal of Geophysical Research*, *114*, A08104. <https://doi.org/10.1029/2009JA014125>
- Matthiä, D., Heber, B., Reitz, G., Sihver, L., Berger, T., & Meier, M. (2009). The ground level event 70 on December 13th, 2006 and related effective doses at aviation altitudes. *Radiation Protection Dosimetry*, *136*(4), 304–310. <https://doi.org/10.1093/rpd/ncp141>
- Matthiä, D., Schaefer, M., Meier, M. M., & M. M. (2015). Economic impact and effectiveness of radiation protection measures in aviation during a ground level enhancement. *Journal of Space Weather and Space Climate*, *5*, A17. <https://doi.org/10.1051/swsc/2015014>
- Mavromichalaki, H., Papaioannou, A., Plainaki, C., Sarlanis, C., Souvatzoglou, G., Gerontidou, M., et al. (2011). Applications and usage of the real-time Neutron Monitor Database. *Advances in Space Research*, *47*(12), 2210–2222.
- Mazur, J. E., Mason, G. M., Looper, M. D., Leske, R. A., & Mewaldt, R. A. (1999). Charge states of solar energetic particles using the geomagnetic cutoff technique: SAMPEX measurements in the 6 November 1997 solar particle event. *Geophysical Research Letters*, *26*, 173–176. <https://doi.org/10.1029/1998GL900075>
- Meier, M. M., & Matthiä, D. (2014). A space weather index for the radiation field at aviation altitudes. *Journal of Space Weather and Space Climate*, *4*, A13. <https://doi.org/10.1041/swsc/2014010>
- Mewaldt, R. A., Looper, M. D., Cohen, C. M. S., Haggerty, D. K., Labrador, A. W., Leske, R. A., et al. (2012). Energy spectra, composition, and other properties of ground-level events during solar cycle 23. *Space Science Reviews*, *171*(1–4), 97–120. <https://doi.org/10.1007/s11214-012-9884-2>
- Miroshnichenko, L. I., de Koning, C. A., & Perez-Enriquez, R. (2000). Large solar event of September 29, 1989: Ten years after. *Space Science Reviews*, *91*, 615–715.
- Miroshnichenko, L. I., Klein, K.-L., Trotter, G., Lantos, P., Vashenyuk, E. V., Balabin, Y. V., & Gvozdevsky, B. B. (2005). Relativistic nucleon and electron production in the 2003 October 28 solar event. *Journal of Geophysical Research*, *110*, A09S08. <https://doi.org/10.1029/2004JA010936>; correction, *Journal of Geophysical Research*, *110*, A11S90. <https://doi.org/10.1029/2005JA011441>
- Mishev, A. L., Kocharov, L. G., & Usoskin, I. G. (2014). Analysis of the ground level enhancement on 17 May 2012 using data from the global neutron monitor network. *Journal of Geophysical Research: Space Physics*, *119*, 670–679. <https://doi.org/10.1002/2013JA019253>
- Mishev, A. L., Usoskin, I. G., & Kovaltsov, G. A. (2013). Neutron monitor yield function: New improved computations. *Journal of Geophysical Research: Space Physics*, *118*, 2783–2788. <https://doi.org/10.1002/jgra.50325>
- Mishev, A. L., Velinov, P. I. Y., Mateev, L., & Tassev, Y. (2011). Ionization effect of solar protons in the Earth atmosphere—Case study of the 20 January 2005 SEP event. *Advances in Space Research*, *48*(7), 1232–1237.
- Núñez, M. (2011). Predicting solar energetic proton events (E > 10 MeV). *Space Weather*, *9*, S07003. <https://doi.org/10.1029/2010SW000640>
- Núñez, M. (2015). Real-time prediction of the occurrence and intensity of the first hours of >100 MeV solar energetic proton events. *Space Weather*, *13*, 807–819. <https://doi.org/10.1002/2015SW001256>

- Oh, S. Y., Yi, Y., Bieber, J. W., Evenson, P., & Kim, Y. K. (2010). Characteristics of solar proton events associated with ground level enhancements. *Journal of Geophysical Research*, *115*, A10107. <https://doi.org/10.1029/2009JA015171>
- Panametrics (1980). GOES D, E, F progress report, Energetic Particle Sensor Dome calibration work (Tech. Rep. PANA-GOESP-CR3). Waltham, MA: Panametrics, Inc. Retrieved from <http://www.ngdc.noaa.gov/stp/satellite/goes/documentation.html>
- Panametrics (1990). Report on the proton calibration of HEPAD SN 002 consisting of HEPAD FAC PN 571774-01, Serial No. 002 at the Alternating Gradient Synchrotron of Brookhaven National Laboratory (Tech. Rep. NXT-CAL-107). Waltham, MA: Panametrics, Inc. Retrieved from <http://www.ngdc.noaa.gov/stp/satellite/goes/documentation.html>
- Panametrics (1995). Calibration report for the EPS Dome Sensor response to protons (Tech. Rep. NXT-CAL-102). Waltham, MA: Panametrics, Inc. Retrieved from <http://www.ngdc.noaa.gov/stp/satellite/goes/documentation.html>
- Plainaki, C., Belov, A., Eroshenko, E., Mavromichalaki, H., & Yanke, V. (2007). Modeling ground level enhancements: Event of 20 January 2005. *Journal of Geophysical Research*, *112*, A04102. <https://doi.org/10.1029/2006JA011926>
- Plainaki, C., Mavromichalaki, H., Belov, A., Eroshenko, E., & Yanke, V. (2009a). Modeling the solar cosmic ray event of 13 December 2006 using ground level neutron monitor data. *Advances in Space Research*, *43*(4), 474–479.
- Plainaki, C., Mavromichalaki, H., Belov, A., Eroshenko, E., & Yanke, V. (2009b). Neutron monitor asymptotic directions of viewing during the event of 13 December 2006. *Advances in Space Research*, *43*(4), 518–522.
- Plainaki, C., Mavromichalaki, H., Laurenza, M., Gerontidou, M., Kanellakopoulos, A., & Storini, M. (2014). The ground-level enhancement of 2012 May 17: Derivation of solar proton event properties through the application of the NMBANGLE PPOLA model. *The Astrophysical Journal*, *785*(2), 160.
- Reames, D. V. (2009). Solar energetic-particle release times in historical ground-level events. *The Astrophysical Journal*, *706*(1), 844–850.
- Rinehart, M. C. (1978). Cerenkov counter for spacecraft application. *Nuclear Instruments and Methods*, *154*(2), 303–316.
- Rodriguez, J. V., Krossschell, J. C., & Green, J. C. (2014). Intercalibration of GOES 8–15 solar proton detectors. *Space Weather*, *12*, 92–109. <https://doi.org/10.1002/2013SW000996>
- Rodriguez, J. V., Onsager, T. G., & Mazur, J. E. (2010). The east-west effect in solar proton flux measurements in geostationary orbit: A new GOES capability. *Geophysical Research Letters*, *37*, L07109. <https://doi.org/10.1029/2010GL042531>
- Rodriguez, J. V., Sandberg, I., Mewaldt, R. A., Daglis, I. A., & Jiggins, P. (2017). Validation of the effect of cross-calibrated GOES solar proton effective energies on derived integral fluxes by comparison with STEREO observations. *Space Weather*, *15*, 290–309. <https://doi.org/10.1002/2016SW001533>
- Sandberg, I., Jiggins, P., Heynderickx, D., & Daglis, I. A. (2014). Cross calibration of NOAA GOES solar proton detectors using corrected NASA IMP-8/GME data. *Geophysical Research Letters*, *41*, 4435–4441. <https://doi.org/10.1002/2014GL060469>
- Sauer, H. H., & Wilkinson, D. C. (2008). Global mapping of ionospheric HF/VHF radio wave absorption due to solar energetic protons. *Space Weather*, *6*, S12002. <https://doi.org/10.1029/2008SW000399>
- Sellers, F. B., & Hanser, F. A. (1996). Design and calibration of the GOES-8 particle sensors: The EPS and HEPAD. In E. R. Washwell (Ed.), *GOES-8 and Beyond, Proc. SPIE* (Vol. 2812, pp. 353–364). Bellingham, WA: International Society for Optical Engineering.
- Shea, M. A., & Smart, D. F. (2012). Space weather and the ground-level solar proton events of the 23rd solar cycle. *Space Science Reviews*, *171*, 161–188.
- Simpson, J. A., Fonger, W., & Treiman, S. B. (1953). Cosmic radiation intensity-time variations and their origin, I. Neutron intensity variation method and meteorological factors. *Physics Review*, *90*(5), 934–950.
- Souvatoglou, G., Papaioannou, A., Mavromichalaki, H., Dimitroulakos, J., & Sarlanis, C. (2014). Optimizing the real-time ground level enhancement alert system based on neutron monitor measurements: Introducing *GLE Alert Plus*. *Space Weather*, *12*, 633–649. <https://doi.org/10.1002/2014SW001102>
- Tylka, A. J., & Dietrich, W. F. (2009). A new and comprehensive analysis of proton spectra in ground-level enhanced (GLE) solar particle events, *Proc. 31st Int'l Cosmic Ray Conf. (Łódź)*, 7–15.
- Usoskin, I. G., Kovaltsov, G. A., Mironova, I. A., Tylka, A. J., & Dietrich, W. F. (2011). Ionization effect of solar particle GLE events in low and middle atmosphere. *Atmospheric Chemistry and Physics*, *11*(5), 1979–1988. <https://doi.org/10.5194/acp-11-1979-2011>
- Zucca, P., Núñez, M., & Klein, K.-L. (2017). Exploring the potential of microwave diagnostics in SEP forecasting: The occurrence of SEP events. *Journal of Space Weather and Space Climate*, *7*, A13. <https://doi.org/10.1051/swsc/2017011>